Search for dark matter annihilations in the center of the Earth with IceCube

Citation for the original published paper (version of record):

N.B. When citing this work, cite the original published paper.

(article starts on next page)

Search for dark matter annihilations in the center of the Earth with IceCube

The IceCube Collaboration

(a complete list of authors can be found at the end of the proceedings)

E-mail: Giovanni.Renzi@ulb.be, Juan.Antonio.Aguilar.Sánchez@ulb.be

The nature of Dark Matter remains one of the most important unresolved questions of fundamental physics. Many models, including the Weakly Interacting Massive Particles (WIMPs), assume Dark Matter to be a particle and predict a weak coupling with Standard Model matter. If Dark Matter particles can scatter off nuclei in the vicinity of a massive object, such as a star or a planet, they may lose kinetic energy and become gravitationally trapped in the center of such objects, including Earth. As Dark Matter accumulates in the center of the Earth, self-annihilation of WIMPs into Standard Model particles can result in an excess of neutrinos coming from the center of the Earth and detectable at the IceCube Neutrino Observatory, situated at the geographic South Pole. A search for excess neutrinos from these annihilations has been performed on 10 years of IceCube data, and results have been interpreted in the context of a number of WIMP annihilation channels $(\chi\chi \rightarrow \tau^+\tau^-/W^+W^-/b\bar{b})$ and masses ranging from 10 GeV to 10 TeV. We present the results from this analysis and compare the outcome with previous searches by other experiments. This analysis yields competitive and world-leading results for masses $m_\chi > 100$ GeV.

Corresponding authors: Giovanni Renzi[1], J. A. Aguilar[1*]

[1] *Université Libre de Bruxelles, Science Faculty CP230, B-1050 Brussels, Belgium*

* Presenter

1. Introduction

Over the last century, an increasing amount of compelling evidence has emerged, indicating that approximately 27% of the Universe and about 85% of its matter content [1] is composed of unknown matter. This elusive form of matter, referred to as *dark matter* (DM), must exhibit a low probability of interaction with ordinary matter.

DM particles, denoted χ, can be captured by the gravitational potential of celestial bodies, such as the Sun or the Earth. This capture occurs through repeated scattering interactions with DM particles in orbits intersecting these celestial objects. As a result of these interactions, dark matter particles can lose energy and fall below the gravitational escape velocity. Over time, this will generate an over abundance of dark matter at the center of the celestial body favoring possible process of self-annihilation and therefore reducing the among to DM particles. The process of DM capturing in Earth was first studied in [2]. The evolution of number density of DM particles, N_χ, will follow the equation that describes the interplay between capturing and annihilation as:

$$\frac{\mathrm{d}N_\chi}{\mathrm{d}t} = C_{\mathrm{C}} - C_{\mathrm{A}}N_\chi^2 - C_{\mathrm{E}}N_\chi. \tag{1}$$

In this equation C_{C} refers to the capture rate and $C_{\mathrm{A}}N_\chi^2 = \Gamma_{\mathrm{A}}$ is the annihilation rate. The third process, represented by $C_{\mathrm{E}}N_\chi$, is the so-called *evaporation*, which describes the process in which after scattering the DM particles gains kinetic energy above the escape velocity and therefore escapes. Evaporation can be ignored for dark matter masses above ~ 12 GeV [3]. The capturing rate, depends on the local DM density, the scattering cross-section, and the chemical composition of the target body. The local halo DM density cannot be stated with certainty and is expected to be in the range $0.1 < \rho_{\mathrm{DM}}/\mathrm{GeV\ cm}^{-3} < 0.5$ [4]. The value assumed conventionally and used for the analysis presented in this work is $\rho_{\mathrm{DM}} = 0.3$ GeV cm^{-3}. Figure 1 shows the Earth's capturing rate assuming the Earth's composition in [5] as function of the DM mass.
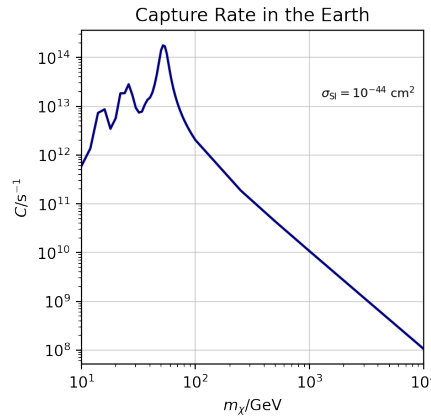

Figure 1: Capture rate as a function of the dark matter particle mass for the spin-independent WIMP-nucleon scattering cross section value $\sigma_{\chi N}^{\mathrm{SI}} = 10^{-44}$ cm^2. The peaks correspond to resonance capture with the most abundant elements on Earth: O, Mg, Si, and Fe. Computed using DarkSusy [6] [7] [8].

The peaks in the capturing rate are due to resonance capture with the most abundant elements on the Earth. Most abundant elements on Earth do not carry spin hence the most relevant scattering

process is the spin-independent dark matter-nucleon scattering, $\sigma_{\chi N}^{\text{SI}}$.

As can be seen in Eq. (1), the annihilation rate depends on the dark matter number density squared, as two dark matter particles are needed for annihilation, as well as the self-annihilation cross-section, usually expressed as a velocity averaged cross-section, $\langle \sigma_{\text{A}} v \rangle$. Equation (1) can be solved and has a solution that can be expressed as:

$$\Gamma_{\text{A}}(t) = \frac{1}{2} C_{\text{C}} \tanh^2 \left(\frac{t}{\tau} \right), \tag{2}$$

where $\tau = (C_{\text{C}} C_{\text{A}})^{-1/2}$ is the time scale for the capture and annihilation processes to reach equilibrium. The equilibrium condition is fulfilled when $t \geq \tau$, so that Eq. (2) becomes $C_{\text{C}} = \frac{1}{2} \Gamma_{\text{A}}$. In this case the annihilation rate reaches its maximum. For typical value of the thermal relic annihilation cross section the Earth is far from equilibrium ($t_{\oplus} \ll \tau$). However, enhancements in the annihilation cross-section such as a nearby clump of DM or a low-velocity Sommerfeld effect, will increase the annihilation rate for the Earth while not for the Sun which is, likely, already in hydrostatic equilibrium [9]. Due to its low escape velocity, Earth capturing is very sensitive to the low tail of the DM velocity distribution. However the low speed distribution is not precisely known, and deviations from the standard halo model could significantly enhance the capturing rate [10].

As DM annihilates, it will produce stable particles, such γ-rays and neutrinos. Given the density of the Earth, only neutrinos can reach the surface and interact in the vicinity of a neutrino telescope. This constitutes the base of the detection principle for indirect searches of dark matter from the center of the Earth.

2. The IceCube Neutrino Observatory

The IceCube Neutrino Observatory [11] is a one-cubic-kilometer neutrino telescope situated at the geographic South Pole. The detector is composed of 5160 photo-multiplier units (DOMs) deployed on 86 strings and is buried in the Antarctic ice-cap between the depths of 1,450 m and 2,450 m. IceCube detects Cherenkov light induced by the passage of superluminal charged leptons and hadrons produced in neutrino interactions in ice. The number of Cherenkov photons and their arrival time is used to reconstruct the direction and energy information of the incoming neutrino. Based on its geometry, IceCube can detect neutrinos with energy ranging from a few GeV to a few PeV. A denser sub-array, *DeepCore* [11], is placed between 2100 m and 2450 m of depth and extends the detection threshold to lower energy neutrinos, between 10 GeV and 100 GeV.

3. Data Selection

Neutrinos produced as by-products of the DM self-annihilation at the center of the Earth, will reach the IceCube detector with vertical up-going directions. Hence, the data selection is designed and optimized to keep vertical tracks. The first step of the processing focuses on reducing the muon atmospheric background events which arrive to the detector with downward going directions. Once data is reduced to an manageable level, we applied a random forest of boosted decision trees (BDTs) to discriminate mis-reconstructed muon events from neutrino events. A random forest assigns to each event a score ranging from -1 (most background-like) to +1 (most signal-like). At this point,
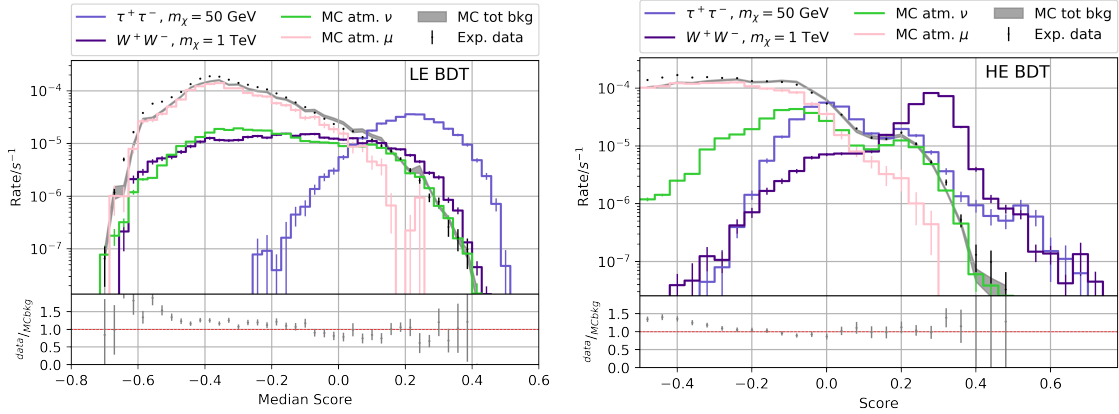
Figure 2: Score distributions for the LE (left) and HE (right) random forests. The baseline LE and HE signal configurations are in light purple and dark purple, respectively. Atmospheric neutrinos and muons are in green and pink respectively. The grey band indicates the total background estimation while the black dots represent the data verification sample.

we can observe differences between the highest and lowest energy signal events: low-energy events appear more like cascade events, mostly comprised in DeepCore; high-energy events consist of kilometer-long tracks. In a intermediate step, a higher-performing but computationally intensive energy reconstruction is applied. The last selection based on the random forest classification is optimized to maximize the sensitivity of the analysis. Two BDT are applied, one which is tuned to select high energy signal, and another one optimized for low energy dark matter masses.

Figure 2 shows the differences in the score distributions for the LE and HE baseline signal configurations for the two random forests.

In this analysis we used 3,619 days of data taking over ten detector seasons from May 2011 to May 2020. A subset of 353 days, taken sparsely over the ten seasons, have been used as a verification dataset along the event selection process. The verification dataset has been omitted from the analysis, leaving a final of 3,266 available days of data.

4. Background and Signal Simulation

Neutrinos from the center of the Earth have an unique direction in IceCube's local coordinate system. There is no other direction in the sky in which IceCube has the same detector response, therefore background estimation techniques, like *on-source/off-source* methods, are not possible. This includes the typical method used in searches for point sources in neutrinos telescopes called right-ascension scrambling, which makes use of the uniform response of the detector in right-ascension due to Earth's rotation. For this reason, this analysis relies on MonteCarlo simulation to estimate the background at a perfect upward going direction. The atmospheric muons generated by cosmic-ray showers are simulated using CORSIKA [12]. The diffuse atmospheric, prompt [13] and astrophysical neutrinos [14] are simulated using two different neutrino generators: GENIE [15] for energies up to 100 GeV and NuGen [16] beyond. The reason for these two simulations is due to the different implementation and energy regime of the neutrino nucleon interaction, with NuGen

4

Table 1: Summary of WIMPs simulation scenarios produced with WimpSim.

Channel	Masses
$\chi\chi \rightarrow \tau^+\tau^-$	[10, 20, 35, 50] GeV
	[100, 250, 500] GeV
	[1, 3, 5, 10] TeV
$\chi\chi \rightarrow W^+W^-$	[100, 250, 500] GeV
	[1, 3, 5, 10] TeV
$\chi\chi \rightarrow b\bar{b}$	[35, 50] GeV
	[100, 250, 500] GeV
	[1, 3, 5, 10] TeV

covering the deep inelastic scattering and GENIE the quasi-elastic interaction. After generating interaction vertexes, all charge particles are then propagated through the detector and their induced Cherenkov light production and detection also simulated.

Neutrinos from the annihilation of DM at the center of the Earth are simulated using the WIMP-sim [17]. Re-weighting of the isotropic simulation from GENIE and NuGen becomes impractical again due to the unique direction in local coordinates of the DM signal. Neutrinos from WIMPSim are generated as coming from the center of the Earth ($\theta = 180°$) and their interaction products are propagated and simulated in the same fashion as astrophysical and atmospheric neutrinos.

We produced simulations over DM particle mass values ranging from 10 GeV to 10 TeV in three annihilation channels: $\chi\chi \rightarrow \tau^+\tau^-/W^+W^-/b\bar{b}$. All the simulated mass-channel configurations are resumed in Table 1. We chose two baseline signal configurations, a low-energy one for $\chi\chi \rightarrow \tau^+\tau^-$, $m_\chi = 50$ GeV, and a high-energy one for $\chi\chi \rightarrow W^+W^-$, $m_\chi = 1$ TeV. As the event selection selects track-like events, only muon neutrinos are considered for these simulations.

5. Analysis Method

We used a binned Poisson likelihood method using as observables the reconstructed energy of the event and their reconstructed zenith angle. The expected signal from DM will arrive from almost vertical directions ($\theta_{rec} \sim 180°$). We produce binned probability density functions (PDFs) over these two observables based on the final distributions obtained in the event selection process after applying a kernel density estimation (KDE) technique to cope with statistical fluctuations due to low statistics. For the LE analysis, we include events with energy in the range 1 GeV $< E_{\text{reco}} < 10^4$ GeV. We found the optimised number of bins at 32×32, for a total of 1024 bins. For the HE analysis, the energy range (in GeV) is $1 < E_{\text{reco}} < 10^5$ and the optimised bins grid is 100×100 for a total of 10^4 bins. For both analyses, the zenith angle range is $160° < \theta_{\text{reco}} < 180°$. The PDFs for the signal and atmospheric background are shown in Figs. 3 and 4 for LE and HE, respectively.

The expected fraction of events in the i-th bin, λ_i, can be expressed as:

$$\lambda_i = \xi S_i + (1 - \xi)B_i, \tag{3}$$

where ξ is the signal fraction and the parameter against with the likelihood is minimized. The background density B_i is composed, likewise, of many different components: atmospheric
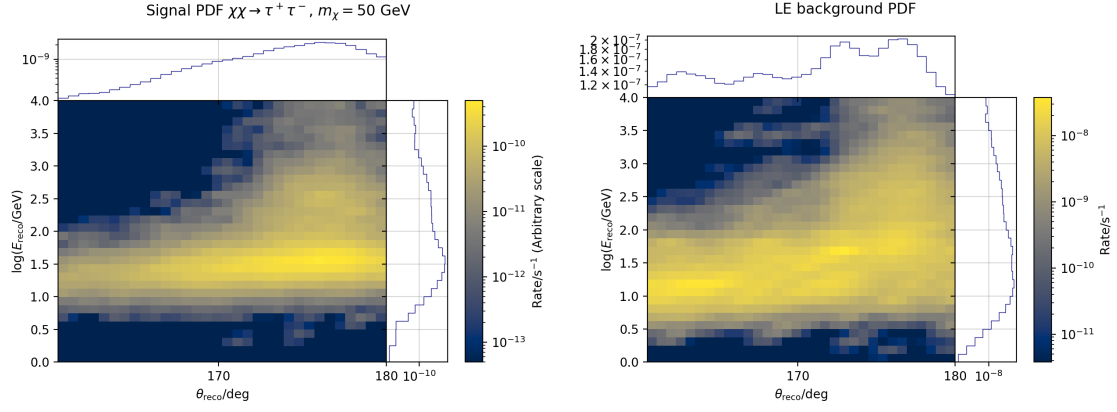
Figure 3: PDFs for the LE analysis. The zenith angle, θ_{reco}, is on the x-axis while the log-energy, $\log(E_{\text{reco}})$, is on the y-axis. The LE signal baseline and the atmospheric background are shown on the left and on the right, respectively.
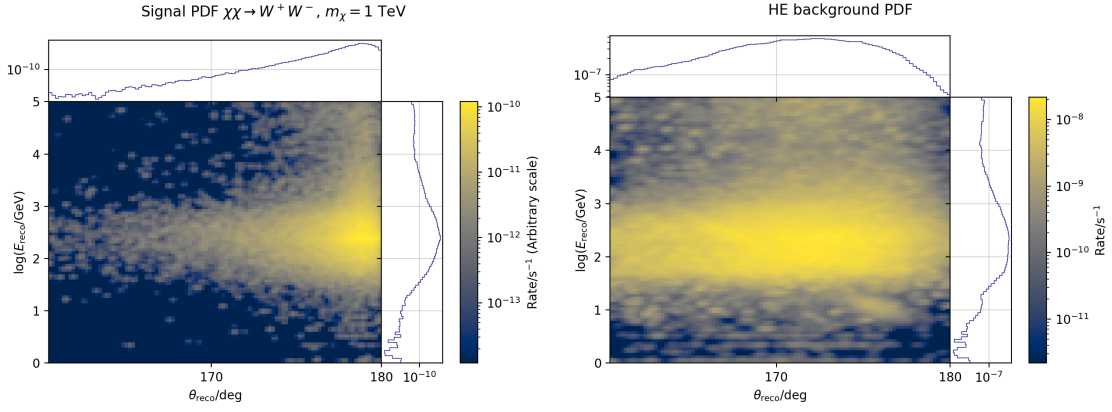

Figure 4: PDFs for the HE analysis. The zenith angle, θ_{reco}, is on the x-axis while the log-energy, $\log E_{\text{reco}}$, is on the y-axis. The LE signal baseline and the atmospheric background are shown on the left and on the right, respectively.

neutrinos and muons, astrophysical neutrinos and prompt neutrinos. Their relative normalization are kept as nuisance parameters in the minimization and expressed as:

$$\lambda_i = \xi S_i + \sum_{j=1}^{n-1} \prod_{k=0}^{j-1} (1 - n_k) n_j B_i^j + \prod_{k=0}^{n-1} (1 - n_k) B_i^n, \tag{4}$$

where n_k refers to the different background event fractions which can be encompassed by $\vec{\eta} = (n_1, ..., n_{n-1})$ and k_i being the observed number of events in the i-th bin. We then search the parameters, ξ, and η that minimize the likelihood:

$$-\log \mathcal{L}(\xi, \vec{\eta}) = \sum_{i}^{N_{bins}} (-k_i \log \lambda_i + \lambda_i). \tag{5}$$
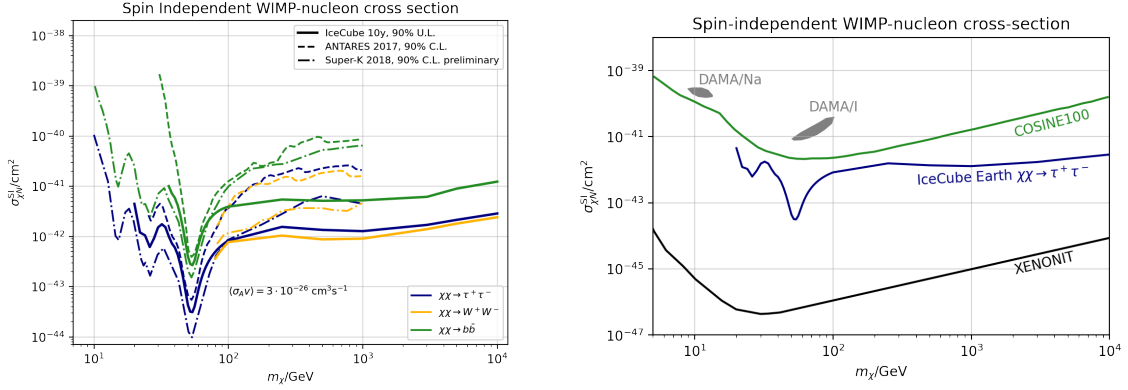
Figure 5: Left: Spin-indenpendent DM-nucleon cross-section 90% C.L. upper limits. Limits in bold are from this analysis, ANTARES (dashed) and Super-Kamiokande (dot-dashed) limits are included. The colour code identifies the annihilation channels, blue for annihilation into $\tau^+\tau^-$, yellow for W^+W^- and green for $b\bar{b}$. Right: Upper limits for this analysis (blue) for the $\chi\chi \to \tau^+\tau^-$ annihilation channel compared to direct detection upper limits from the crystal experiments DAMA/LIBRA [22] (grey areas) and COSINE100 [23] (green) and from XENON1T [24] (black).

In order to perform an hypothesis testing, we define a test-statistics as the likelihood ratio:

$$t_\xi = 2\log\frac{\mathcal{L}(\xi, \hat{\hat{\vec{\eta}}})}{\mathcal{L}(\hat{\xi}, \hat{\vec{\eta}})} = 2(\log\mathcal{L}(\xi, \hat{\hat{\vec{\eta}}}) - \log\mathcal{L}(\hat{\xi}, \hat{\vec{\eta}})), \tag{6}$$

where $\hat{\xi}$, $\hat{\eta}$ are the estimated parameters that minimize the likelihood, $\mathcal{L}(\hat{\xi}, \hat{\vec{\eta}})$, and $\hat{\hat{\eta}}$ is the value of η that minimizes the likelihood for any given value of ξ. To claim a discovery we estimate the agreement with respect to the null hypothesis $\xi = 0$, and so the test-statistics is defined as t_0. Assuming Wilk's theorem [18, 19] and that the distribution of t_0 under sample of null-hypothesis follows a χ^2 distribution, we can estimate the p-value in terms of number of sigmas z-score as $z - \text{score} = \sqrt{t_0}$.

6. Results and Conclusions

We found no significant excess over all channels and masses tested. The highest pre-trial significance belongs to the HE analysis at 1.94σ for the channel $\chi\chi \to b\bar{b}$ and mass $m_\chi = 250$ GeV. The trial factor correction gives a post-trial significance of 1.06σ. Upper limits in the signal fraction of events ξ, can be converted into upper limits on the spin-independent DM-nucleon cross-section $\sigma_{\chi N}^{\text{SI}}$ after assuming a value on the DM self-annihilation cross-section.

The 90% C.L. upper limits for $\sigma_{\chi N}^{\text{SI}}$ are presented in Fig. 5, compared to results from the other neutrino telescopes ANTARES [20] and Super-Kamiokande [21].

Although optimized for signals from WIMP-like particles, the results from this analysis can also be re-casted to set limits on different DM models. An example can be found in [25], where limits on the coupling constant of the effective field theory of dark matter [26] were computed.

With the installation of the IceCube Upgrade [27] a significant improvement in IceCube's sensitivity can be expected, especially in the low-mass region.

7

References

[1] **Planck** Collaboration, N. Aghanim *et al. Astron. Astrophys.* **641** (2020) A6.

[2] A. Gould *Astrophys. J.* **321** (Oct., 1987) 571.

[3] R. Garani and S. Palomares-Ruiz *JCAP* **2022** no. 05, (May, 2022) 042.

[4] L. Necib, M. Lisanti, and V. A. Belokurov *Astrophys. J.* **874** (2019) .

[5] W. McDonough *Treatise on Geochemistry* **2** (11, 2003) 547–568.

[6] T. Bringmann *et al. JCAP* **2018** (02, 2018) .

[7] P. Gondolo *et al. JCAP* **2004** (06, 2004) .

[8] J. Edsjö *et al.*, "Darksusy, http://www.darksusy.org.".

[9] C. Delaunay, P. J. Fox, and G. Perez *JHEP* **2009** no. 05, (May, 2009) 099.

[10] T. Bruch *et al. Physics Letters B* **674** no. 4, (2009) 250–256.

[11] **IceCube** Collaboration, M. G. Aartsen *et al. JINST* **12** no. 03, (2017) P03012.

[12] D. Heck *et al. FZKA* **6019** (1998) .

[13] R. Enberg, M. H. Reno, and I. Sarcevic *Phys. Rev. D* **78** (Aug, 2008) 043005.

[14] **IceCube** Collaboration, R. Abbasi *et al. Astrophys. J.* **928** no. 1, (2022) 50.

[15] C. Andreopoulos *et al. arXiv e-prints* (10, 2015) .

[16] A. Gazizov and M. Kowalski *Computer Physics Communications* **172** no. 3, (2005) 203–213.

[17] J. Edsjö, J. Elevant, and C. Niblaeus *WimpSim Neutrino Monte Carlo, http://wimpsim.astroparticle.se/* .

[18] S. S. Wilks *The Annals of Mathematical Statistics* **9** (1938) 60–62.

[19] H. Chernoff *Annals of Mathematical Statistics* **25** (1954) .

[20] **ANTARES** Collaboration, A. Albert *et al. Phys. Dark Univ.* **16** (2017) 41–48.

[21] **Super-Kamiokande** Collaboration, P. Mijakowski *J. Phys.: Conf. Ser.* **1342** (Jan, 2020) 012075.

[22] R. Bernabei *et al. Universe* **4** no. 11, (2018) 116.

[23] G. Adhikari *et al. Phys. Rev. Lett.* **123** (07, 2019) .

[24] **XENON** Collaboration, E. Aprile *et al. Phys. Rev. Lett.* **122** no. 14, (2019) 141301.

[25] G. Renzi, *Search for dark matter annihilation in the center of the Earth with ten years of IceCube data.* PhD thesis, Université Libre de Bruxelles, 2022.

[26] R. Catena *JCAP* **2017** no. 01, (Jan, 2017) 059–059.

[27] **IceCube** Collaboration, A. Ishihara *PoS* **ICRC2019** (2021) 1031.

Full Author List: IceCube Collaboration

R. Abbasi[17], M. Ackermann[63], J. Adams[18], S. K. Agarwalla[40, 64], J. A. Aguilar[12], M. Ahlers[22], J.M. Alameddine[23], N. M. Amin[44], K. Andeen[42], G. Anton[26], C. Argüelles[14], Y. Ashida[53], S. Athanasiadou[63], S. N. Axani[44], X. Bai[50], A. Balagopal V.[40], M. Baricevic[40], S. W. Barwick[30], V. Basu[40], R. Bay[8], J. J. Beatty[20, 21], J. Becker Tjus[11, 65], J. Beise[61], C. Bellenghi[27], C. Benning[1], S. BenZvi[52], D. Berley[19], E. Bernardini[48], D. Z. Besson[36], E. Blaufuss[19], S. Blot[63], F. Bontempo[31], J. Y. Book[14], C. Boscolo Meneguolo[48], S. Böser[41], O. Botner[61], J. Böttcher[1], E. Bourbeau[22], J. Braun[40], B. Brinson[6], J. Brostean-Kaiser[63], R. T. Burley[2], R. S. Busse[43], D. Butterfield[40], M. A. Campana[49], K. Carloni[14], E. G. Carnie-Bronca[2], S. Chattopadhyay[40, 64], N. Chau[12], C. Chen[6], Z. Chen[55], D. Chirkin[40], S. Choi[56], B. A. Clark[19], L. Classen[43], A. Coleman[61], G. H. Collin[15], A. Connolly[20, 21], J. M. Conrad[15], P. Coppin[13], P. Correa[13], D. F. Cowen[59, 60], P. Dave[6], C. De Clercq[13], J. J. DeLaunay[58], D. Delgado[14], S. Deng[1], K. Deoskar[54], A. Desai[40], P. Desiati[40], K. D. de Vries[13], G. de Wasseige[37], T. DeYoung[24], A. Diaz[15], J. C. Díaz-Vélez[40], M. Dittmer[43], A. Domi[26], H. Dujmovic[40], M. A. DuVernois[40], T. Ehrhardt[41], P. Eller[27], E. Ellinger[62], S. El Mentawi[1], D. Elsässer[23], R. Engel[31, 32], H. Erpenbeck[40], J. Evans[19], P. A. Evenson[44], K. L. Fan[19], K. Fang[40], K. Farrag[16], A. R. Fazely[7], A. Fedynitch[57], N. Feigl[10], S. Fiedlschuster[26], C. Finley[54], L. Fischer[63], D. Fox[59], A. Franckowiak[11], A. Fritz[41], P. Fürst[1], J. Gallagher[39], E. Ganster[1], A. Garcia[14], L. Gerhardt[9], A. Ghadimi[58], C. Glaser[61], T. Glauch[27], T. Glüsenkamp[26, 61], N. Goehlke[32], J. G. Gonzalez[44], S. Goswami[58], D. Grant[24], S. J. Gray[19], O. Gries[1], S. Griffin[40], S. Griswold[52], K. M. Groth[22], C. Günther[1], P. Gutjahr[23], C. Haack[26], A. Hallgren[61], R. Halliday[24], L. Halve[1], F. Halzen[40], H. Hamdaoui[55], M. Ha Minh[27], K. Hanson[40], J. Hardin[15], A. A. Harnisch[24], P. Hatch[33], A. Haungs[31], K. Helbing[62], J. Hellrung[11], F. Henningsen[27], L. Heuermann[1], N. Heyer[61], S. Hickford[62], A. Hidvegi[54], C. Hill[16], G. C. Hill[2], K. D. Hoffman[19], S. Hori[40], K. Hoshina[40, 66], W. Hou[31], T. Huber[31], K. Hultqvist[54], M. Hünnefeld[23], R. Hussain[40], K. Hymon[23], S. In[56], A. Ishihara[16], M. Jacquart[40], O. Janik[1], M. Jansson[54], G. S. Japaridze[5], M. Jeong[56], M. Jin[14], B. J. P. Jones[4], D. Kang[31], W. Kang[56], X. Kang[49], A. Kappes[43], D. Kappesser[41], L. Kardum[23], T. Karg[63], M. Karl[27], A. Karle[40], U. Katz[26], M. Kauer[40], J. L. Kelley[40], A. Khatee Zathul[40], A. Kheirandish[34, 35], J. Kiryluk[55], S. R. Klein[8, 9], A. Kochocki[24], R. Koirala[44], H. Kolanoski[10], T. Kontrimas[27], L. Köpke[41], C. Kopper[26], D. J. Koskinen[22], P. Koundal[31], M. Kovacevich[49], M. Kowalski[10, 63], T. Kozynets[22], J. Krishnamoorthi[40, 64], K. Kruiswijk[37], E. Krupczak[24], A. Kumar[63], E. Kun[11], N. Kurahashi[49], N. Lad[63], C. Lagunas Gualda[63], M. Lamoureux[37], M. J. Larson[19], S. Latseva[1], F. Lauber[62], J. P. Lazar[14, 40], J. W. Lee[56], K. Leonard DeHolton[60], A. Leszczyńska[44], M. Lincetto[11], Q. R. Liu[40], M. Liubarska[25], E. Lohfink[41], C. Love[49], C. J. Lozano Mariscal[43], L. Lu[40], F. Lucarelli[28], W. Luszczak[20, 21], Y. Lyu[8, 9], J. Madsen[40], K. B. M. Mahn[24], Y. Makino[40], E. Manao[27], S. Mancina[40, 48], W. Marie Sainte[40], I. C. Mariş[12], S. Marka[46], Z. Marka[46], M. Marsee[58], I. Martinez-Soler[14], R. Maruyama[45], F. Mayhew[24], T. McElroy[25], F. McNally[38], J. V. Mead[22], K. Meagher[40], S. Mechbal[63], A. Medina[21], M. Meier[16], Y. Merckx[13], L. Merten[11], J. Micallef[24], J. Mitchell[7], T. Montaruli[28], R. W. Moore[25], Y. Morii[16], R. Morse[40], M. Moulai[40], T. Mukherjee[31], R. Naab[63], R. Nagai[16], M. Nakos[40], U. Naumann[62], J. Necker[63], A. Negi[4], M. Neumann[43], H. Niederhausen[24], M. U. Nisa[24], A. Noell[1], A. Novikov[44], S. C. Nowicki[24], A. Obertacke Pollmann[16], V. O'Dell[40], M. Oehler[31], B. Oeyen[29], A. Olivas[19], R. Ørsøe[27], J. Osborn[40], E. O'Sullivan[61], H. Pandya[44], N. Park[33], G. K. Parker[4], E. N. Paudel[44], L. Paul[42, 50], C. Pérez de los Heros[61], J. Peterson[40], S. Philippen[1], A. Pizzuto[40], M. Plum[50], A. Pontén[61], Y. Popovych[41], M. Prado Rodriguez[40], B. Pries[24], R. Procter-Murphy[19], G. T. Przybylski[9], C. Raab[37], J. Rack-Helleis[41], K. Rawlins[3], Z. Rechav[40], A. Rehman[44], P. Reichherzer[11], G. Renzi[12], E. Resconi[27], S. Reusch[63], W. Rhode[23], B. Riedel[40], A. Rifaie[1], E. J. Roberts[2], S. Robertson[8, 9], S. Rodan[56], G. Roellinghoff[56], M. Rongen[26], C. Rott[53, 56], T. Ruhe[23], L. Ruohan[27], D. Ryckbosch[29], I. Safa[14, 40], J. Saffer[32], D. Salazar-Gallegos[24], P. Sampathkumar[31], S. E. Sanchez Herrera[24], A. Sandrock[62], M. Santander[58], S. Sarkar[25], S. Sarkar[47], J. Savelberg[1], P. Savina[40], M. Schaufel[1], H. Schieler[31], S. Schindler[26], L. Schlickmann[1], B. Schlüter[43], F. Schlüter[12], N. Schmeisser[62], T. Schmidt[19], J. Schneider[26], F. G. Schröder[31, 44], L. Schumacher[26], G. Schwefer[1], S. Sclafani[19], D. Seckel[44], M. Seikh[36], S. Seunarine[51], R. Shah[49], A. Sharma[61], S. Shefali[32], N. Shimizu[16], M. Silva[40], B. Skrzypek[14], B. Smithers[4], R. Snihur[40], J. Soedingrekso[23], A. Søgaard[22], D. Soldin[32], P. Soldin[1], G. Sommani[11], C. Spannfellner[27], G. M. Spiczak[51], C. Spiering[63], M. Stamatikos[21], T. Stanev[44], T. Stezelberger[9], T. Stürwald[62], T. Stuttard[22], G. W. Sullivan[19], I. Taboada[6], S. Ter-Antonyan[7], M. Thiesmeyer[1], W. G. Thompson[14], J. Thwaites[40], S. Tilav[44], K. Tollefson[24], C. Tönnis[56], S. Toscano[12], D. Tosi[40], A. Trettin[63], C. F. Tung[6], R. Turcotte[31], J. P. Twagirayezu[24], B. Ty[40], M. A. Unland Elorrieta[43], A. K. Upadhyay[40, 64], K. Upshaw[7], N. Valtonen-Mattila[61], J. Vandenbroucke[40], N. van Eijndhoven[13], D. Vannerom[15], J. van Santen[63], J. Vara[43], J. Veitch-Michaelis[40], M. Venugopal[31], M. Vereecken[37], S. Verpoest[44], D. Veske[46], A. Vijai[19], C. Walck[54], C. Weaver[24], P. Weigel[15], A. Weindl[31], J. Weldert[60], C. Wendt[40], J. Werthebach[23], M. Weyrauch[31], N. Whitehorn[24], C. H. Wiebusch[1], N. Willey[24], D. R. Williams[58], L. Witthaus[23], A. Wolf[1], M. Wolf[27], G. Wrede[26], X. W. Xu[7], J. P. Yanez[25], E. Yildizci[40], S. Yoshida[16], R. Young[36], F. Yu[14], S. Yu[24], T. Yuan[40], Z. Zhang[55], P. Zhelnin[14], M. Zimmerman[40]

[1] III. Physikalisches Institut, RWTH Aachen University, D-52056 Aachen, Germany

[2] Department of Physics, University of Adelaide, Adelaide, 5005, Australia

[3] Dept. of Physics and Astronomy, University of Alaska Anchorage, 3211 Providence Dr., Anchorage, AK 99508, USA

[4] Dept. of Physics, University of Texas at Arlington, 502 Yates St., Science Hall Rm 108, Box 19059, Arlington, TX 76019, USA

[5] CTSPS, Clark-Atlanta University, Atlanta, GA 30314, USA

[6] School of Physics and Center for Relativistic Astrophysics, Georgia Institute of Technology, Atlanta, GA 30332, USA

[7] Dept. of Physics, Southern University, Baton Rouge, LA 70813, USA

[8] Dept. of Physics, University of California, Berkeley, CA 94720, USA

[9] Lawrence Berkeley National Laboratory, Berkeley, CA 94720, USA

[10] Institut für Physik, Humboldt-Universität zu Berlin, D-12489 Berlin, Germany

[11] Fakultät für Physik & Astronomie, Ruhr-Universität Bochum, D-44780 Bochum, Germany

[12] Université Libre de Bruxelles, Science Faculty CP230, B-1050 Brussels, Belgium

[13] Vrije Universiteit Brussel (VUB), Dienst ELEM, B-1050 Brussels, Belgium

[14] Department of Physics and Laboratory for Particle Physics and Cosmology, Harvard University, Cambridge, MA 02138, USA

[15] Dept. of Physics, Massachusetts Institute of Technology, Cambridge, MA 02139, USA

[16] Dept. of Physics and The International Center for Hadron Astrophysics, Chiba University, Chiba 263-8522, Japan

[17] Department of Physics, Loyola University Chicago, Chicago, IL 60660, USA

[18] Dept. of Physics and Astronomy, University of Canterbury, Private Bag 4800, Christchurch, New Zealand

[19] Dept. of Physics, University of Maryland, College Park, MD 20742, USA

[20] Dept. of Astronomy, Ohio State University, Columbus, OH 43210, USA

[21] Dept. of Physics and Center for Cosmology and Astro-Particle Physics, Ohio State University, Columbus, OH 43210, USA

[22] Niels Bohr Institute, University of Copenhagen, DK-2100 Copenhagen, Denmark

[23] Dept. of Physics, TU Dortmund University, D-44221 Dortmund, Germany

[24] Dept. of Physics and Astronomy, Michigan State University, East Lansing, MI 48824, USA

[25] Dept. of Physics, University of Alberta, Edmonton, Alberta, Canada T6G 2E1

[26] Erlangen Centre for Astroparticle Physics, Friedrich-Alexander-Universität Erlangen-Nürnberg, D-91058 Erlangen, Germany

[27] Technical University of Munich, TUM School of Natural Sciences, Department of Physics, D-85748 Garching bei München, Germany

[28] Département de physique nucléaire et corpusculaire, Université de Genève, CH-1211 Genève, Switzerland

[29] Dept. of Physics and Astronomy, University of Gent, B-9000 Gent, Belgium

[30] Dept. of Physics and Astronomy, University of California, Irvine, CA 92697, USA

[31] Karlsruhe Institute of Technology, Institute for Astroparticle Physics, D-76021 Karlsruhe, Germany

[32] Karlsruhe Institute of Technology, Institute of Experimental Particle Physics, D-76021 Karlsruhe, Germany

[33] Dept. of Physics, Engineering Physics, and Astronomy, Queen's University, Kingston, ON K7L 3N6, Canada

[34] Department of Physics & Astronomy, University of Nevada, Las Vegas, NV, 89154, USA

[35] Nevada Center for Astrophysics, University of Nevada, Las Vegas, NV 89154, USA

[36] Dept. of Physics and Astronomy, University of Kansas, Lawrence, KS 66045, USA

[37] Centre for Cosmology, Particle Physics and Phenomenology - CP3, Université catholique de Louvain, Louvain-la-Neuve, Belgium

[38] Department of Physics, Mercer University, Macon, GA 31207-0001, USA

[39] Dept. of Astronomy, University of Wisconsin–Madison, Madison, WI 53706, USA

[40] Dept. of Physics and Wisconsin IceCube Particle Astrophysics Center, University of Wisconsin–Madison, Madison, WI 53706, USA

[41] Institute of Physics, University of Mainz, Staudinger Weg 7, D-55099 Mainz, Germany

[42] Department of Physics, Marquette University, Milwaukee, WI, 53201, USA

[43] Institut für Kernphysik, Westfälische Wilhelms-Universität Münster, D-48149 Münster, Germany

[44] Bartol Research Institute and Dept. of Physics and Astronomy, University of Delaware, Newark, DE 19716, USA

[45] Dept. of Physics, Yale University, New Haven, CT 06520, USA

[46] Columbia Astrophysics and Nevis Laboratories, Columbia University, New York, NY 10027, USA

[47] Dept. of Physics, University of Oxford, Parks Road, Oxford OX1 3PU, United Kingdom

[48] Dipartimento di Fisica e Astronomia Galileo Galilei, Università Degli Studi di Padova, 35122 Padova PD, Italy

[49] Dept. of Physics, Drexel University, 3141 Chestnut Street, Philadelphia, PA 19104, USA

[50] Physics Department, South Dakota School of Mines and Technology, Rapid City, SD 57701, USA

[51] Dept. of Physics, University of Wisconsin, River Falls, WI 54022, USA

[52] Dept. of Physics and Astronomy, University of Rochester, Rochester, NY 14627, USA

[53] Department of Physics and Astronomy, University of Utah, Salt Lake City, UT 84112, USA

[54] Oskar Klein Centre and Dept. of Physics, Stockholm University, SE-10691 Stockholm, Sweden

[55] Dept. of Physics and Astronomy, Stony Brook University, Stony Brook, NY 11794-3800, USA

[56] Dept. of Physics, Sungkyunkwan University, Suwon 16419, Korea

[57] Institute of Physics, Academia Sinica, Taipei, 11529, Taiwan

[58] Dept. of Physics and Astronomy, University of Alabama, Tuscaloosa, AL 35487, USA

[59] Dept. of Astronomy and Astrophysics, Pennsylvania State University, University Park, PA 16802, USA

[60] Dept. of Physics, Pennsylvania State University, University Park, PA 16802, USA

[61] Dept. of Physics and Astronomy, Uppsala University, Box 516, S-75120 Uppsala, Sweden

[62] Dept. of Physics, University of Wuppertal, D-42119 Wuppertal, Germany

[63] Deutsches Elektronen-Synchrotron DESY, Platanenallee 6, 15738 Zeuthen, Germany

[64] Institute of Physics, Sachivalaya Marg, Sainik School Post, Bhubaneswar 751005, India

[65] Department of Space, Earth and Environment, Chalmers University of Technology, 412 96 Gothenburg, Sweden

[66] Earthquake Research Institute, University of Tokyo, Bunkyo, Tokyo 113-0032, Japan

Acknowledgements

10

POS(ICRC2023)1393